5 Optimization of Helical Orbits

5.1 Separation During the Low-β Squeeze

At the injection energy of 150 GeV separation of the p-pbar orbits is controlled using a small sub-set of the 12 separators available in the machine. In the baseline Run II helix design only the B17(H) and C17(V) modules are used. By also including the B11(H) and C49(V) separators in early 2002 it was found possible to increase the proton intensity by 50% without adversely impacting the pbar lifetime. The majority of beam separation in the ring in this case is still determined by the B17 and C17 settings. The horizontal B17 gradients, in particular, are constrained by the aperture at the F0 lambertson, and their polarity is defined by the orientation of the pbar orbit, which must be to the outside of the ring at F0 to match the strengths of the pbar kickers.

Shortcomings in generating the helix become apparent during acceleration to 1 TeV. A particle loss of about 15% is observed during the second half of the ramp up to flattop. One possible explanation is that this results from the enhancement in beam-beam interactions as the beam separation decreases. For Gaussian transverse particle distributions the rms beam extent can be characterized in terms of the 95%, normalized emittance ε_N, and 95% momentum spread δ_{95} as:

$$\sigma(E) = \sqrt{\beta\varepsilon_N / 6\gamma + \left(\eta\delta_{95}(E) / 2\right)^2}$$

where γ is the relativistic factor E/m, and the momentum spread δ_{95} diminishes with energy according to $E^{-0.75}$. As energy increases, then, the betatron portion of the beam size shrinks only as quickly as $E^{-0.5}$, and the synchrotron contribution varies as $E^{-0.75}$. The angle kick from an electrostatic separator module, by contrast, falls off significantly faster than the beam size, as 1/E. From 150 GeV up to ~500 GeV a constant beam separation, as measured in units of σ, can be maintained by appropriate increases in the separator voltages. Beyond this point, though, the gradients are fixed at their maximum values, which is ~40 kV/cm, with the result that the beam separation, whether measured in σ's of separation or mm's, steadily decreases through the remainder of the acceleration ramp up to flattop at 1 TeV.

The separator settings currently remain unchanged at 1 TeV from the injection optics of Step #1 through to Step #12 ($\beta^* = 0.50$ m). A further decline in beam lifetime then develops during the transformation from the injection helix at Step #12 over to the collision helix at Step #13. This problem arises because to reach the collision helix the horizontal orbits must, in effect, be reversed. During collisions the horizontal orientation of the pbar orbit is determined by the requirements of the D0 Forward Pointing Detectors (Roman Pots). The D0 experiment wants this trajectory to be to the inside of the ring at C49 and to the outside at D11. This is opposite to the pbar's orbit orientation at injection and, so, not surprisingly, the collision helix also reverses the pbar horizontal offset at F0.

The transformation from injection to collision helices is very difficult to accomplish in a smooth fashion with the existing separator configuration. The manipulation requires that at the very least the B17 separators must switch polarity. Since it is B17 that also

provides the bulk of the horizontal separation in the injection helix, during the stage in the transition when the B17 gradient passes through zero there is a tendency for the beam separation to collapse horizontally.

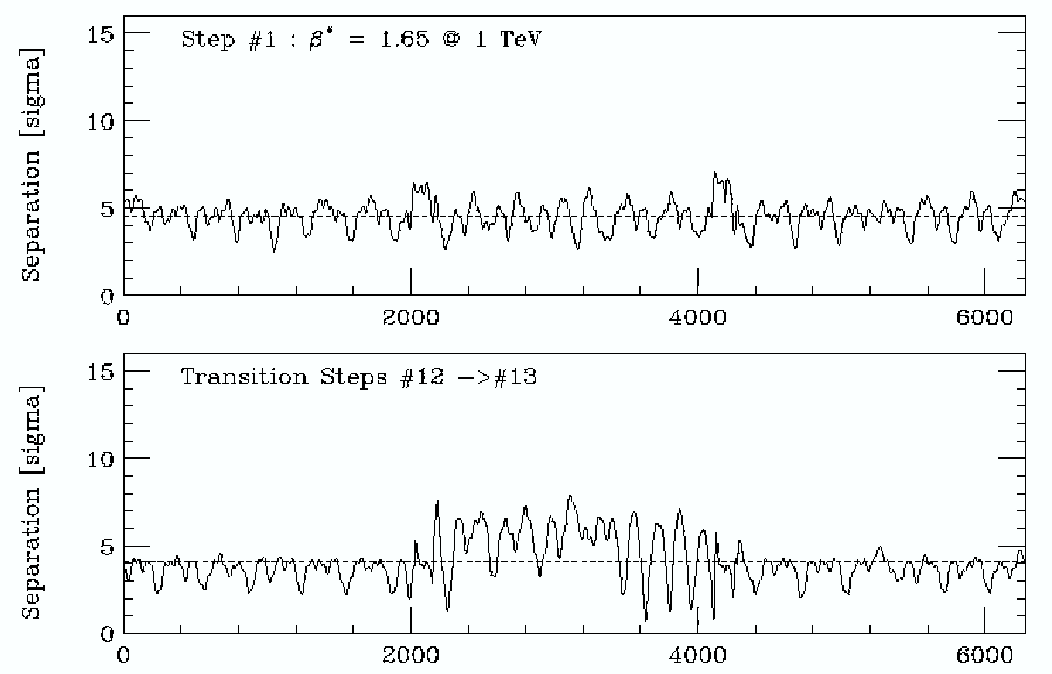

Figure 1. Beam-beam separation at trouble stages of the low-β squeeze in the baseline Run II helix configuration, in units of the rms transverse beam size, for p and pbar beams of 20π μm emittance (95%, normalized) and δp/p = 3.38E-4 (95% at 1 TeV). The top figure corresponds to the injection helix at Step #1, with an average separation $<\sigma_S>$ = 4.5. The lower figure is a snapshot taken mid-way between Steps #12 (β* = 0.50m) and #13 (β* = 0.45m). The average separation here is just $<\sigma_S>$ = 3.8, with several locations having σ_S ~1, and at the worst point separation is only σ_{min} = 0.68.

Some improvements have been accomplished in the smoothing of this process, and thereby improving beam lifetime, by breaking up the step #12→13 transition into several sub-steps and implementing additional separator bumps at each stage. Nevertheless, this remains a problem area and the accepted operational procedure is simply to slam the separator voltages through this transition as quickly as possible. These two problem features inherent to the baseline helix solution – the poor separation at flattop and collapse of horizontal separation during the injection-collision transformation –are clearly illustrated in Fig. 1.

Step #1 Separator Gradients @ 1 TeV (kV/cm)					
Horizontal			Vertical		
A49	1	0.0	A49	2	0.0
B11	2	0.0	B11	1	-40.000
B17	4	40.000			
			C17	4	-40.000
C49	1	40.000	C49	2	-27.627
D11	2	-40.000	D11	1	27.627
D48	1	-5.920			
			A17	1	-40.000

Step #15 Separator Gradients @ Collision (kV/cm)					
Horizontal			Vertical		
A49	1	40.000	A49	2	-32.691
B11	2	40.000	B11	1	-40.000
B17	4	-19.042			
			C17	4	24.353
C49	1	37.070	C49	2	-32.796
D11	2	-34.657	D11	1	40.000
D48	1	-5.920			
			A17	1	-16.354

Table 1. Revised separator gradients at the beginning of the low-β squeeze (top) and at collisions (bottom). At step #1 the B17 and C17 entries are highlighted to emphasize that these separators must switch polarity for collisions. During collisions at step #15 the short-arc vertical B11, C17, and C49 gradients listed are the opposite polarity to those in the current collision helix.

The challenge then is to search for a new separator solution that matches to the optimal injection helix at 150 GeV but improves the p-pbar separation during the ramp from 500 GeV→1 TeV. Further, this solution must transform smoothly, without loss of beam separation, over to the collision helix. Since the Tevatron ramp is long (~80 secs) it is conceivable that the injection-collision transition could even occur partially during acceleration.

One possible separator configuration currently being explored attempts to address both of the squeeze problem stages. By expanding the set of separators used at injection to include essentially all 12 of those available in the ring, separation at flattop can be increased to $\langle\sigma_S\rangle = 6.6$. This is a 47% increase over the current Run II injection helix value at 1 TeV. In the attempt to transform smoothly from here to the collision helix it was found that the process could be eased by reversing the polarities of the short-arc vertical separators in the collision helix definition. Since these 3 separators create a closed 3-bump at collision, switching their polarities has no impact on the magnitude of beam separation at Step #15. As β* is lowered at each stage of the squeeze the phase separation between separators continually changes as the machine gets re-tuned. This characteristic can be used to advantage to further smooth the injection-collision transition

by extending the process over several steps in the squeeze, making small adjustments to the separator gradients at each stage while also optimizing beam separation.

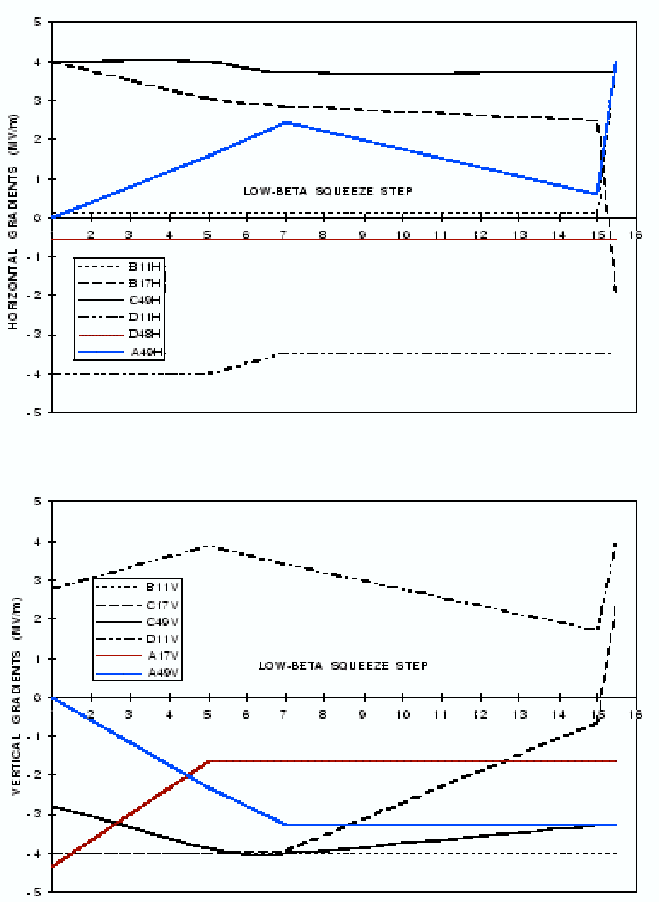

Figure 2. Separator gradients from the injection helix at Step #1 through to collisions. Beyond Step #7 the gradients of 6 of the 12 separators are fixed at their collision helix values. At Step #15 ($\beta^* = 0.35$m) the gradients are shown for separated beams and then the linear ramp of six of the separators to bring the beams into collision. During this stage the B17 and C17 gradients switch polarities.

The separator gradients for this new helix are listed in Table 1 for just Step #1 and Step #15, and their evolution over the entire low−β squeeze is illustrated in Fig. 2. The evolution of the gradients has not yet been completely optimized. Average beam separation was maximized at Steps #1, #5, #7, and #15 ($\beta^* = 0.35$m, but with separated beams). Separator gradients for the other steps in the squeeze were then obtained simply by linear interpolation. Even so, the transition from injection to collision helices is remarkably smooth and maintains ample beam separation throughout the process. Separation increases steadily from $\langle\sigma_S\rangle = 6.6$ at Step #1, and from Step #3 onwards is never less than $\langle\sigma_S\rangle = 7.0$. The separations at a few of the steps in the low−β squeeze are

shown in Fig. 3, and the process of bringing the beams into collisions at Step #15 is illustrated in Fig. 4.

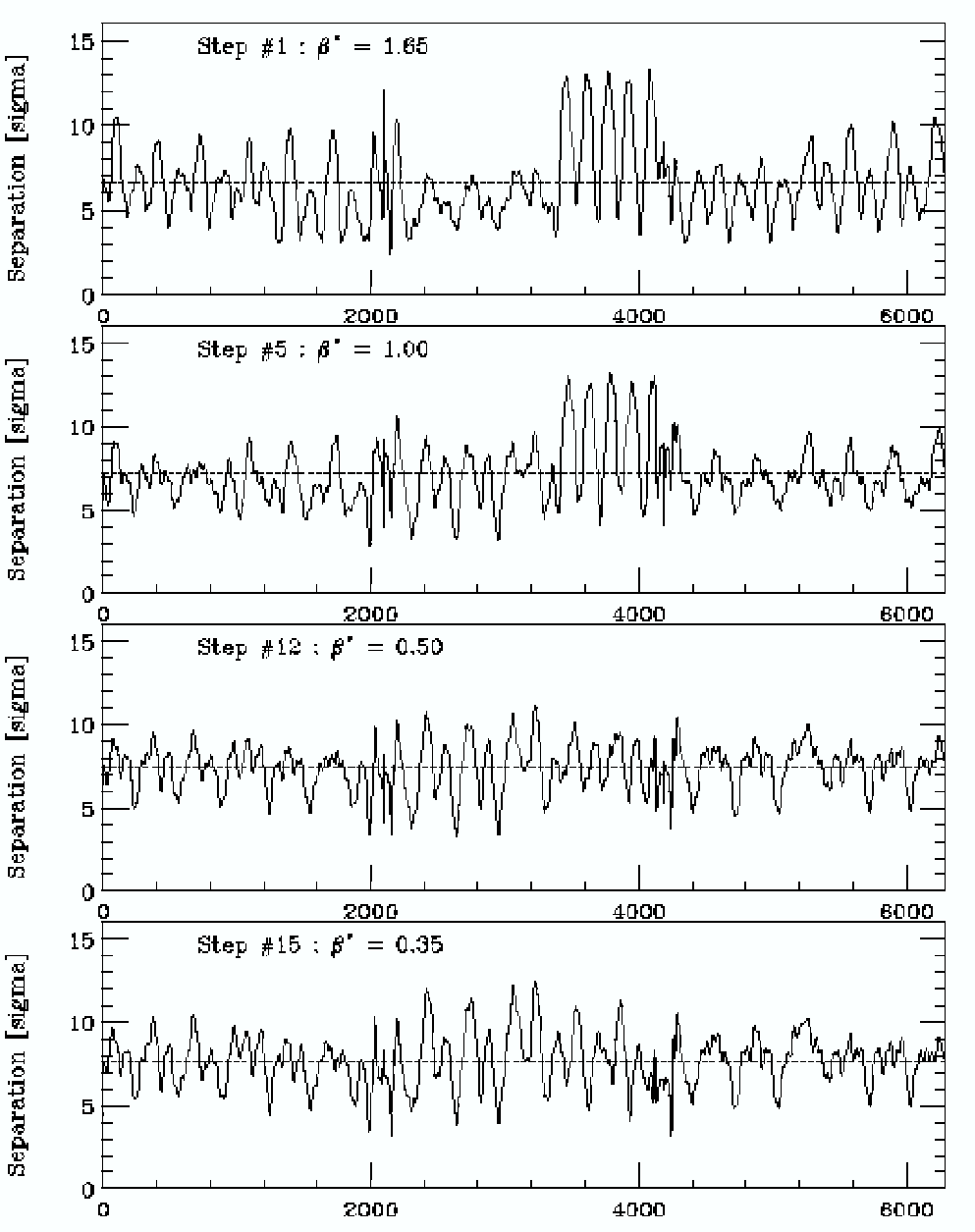

Figure 3. Samplings from the transition between the injection helix (top) through to the collision helix orientation at Step #15 (bottom, prior to the final separator ramp bringing beams into collision). Average separation at these 4 stages are, top to bottom, $\langle\sigma_S\rangle$ = 6.6, 7.2, 7.4, and 7.7.

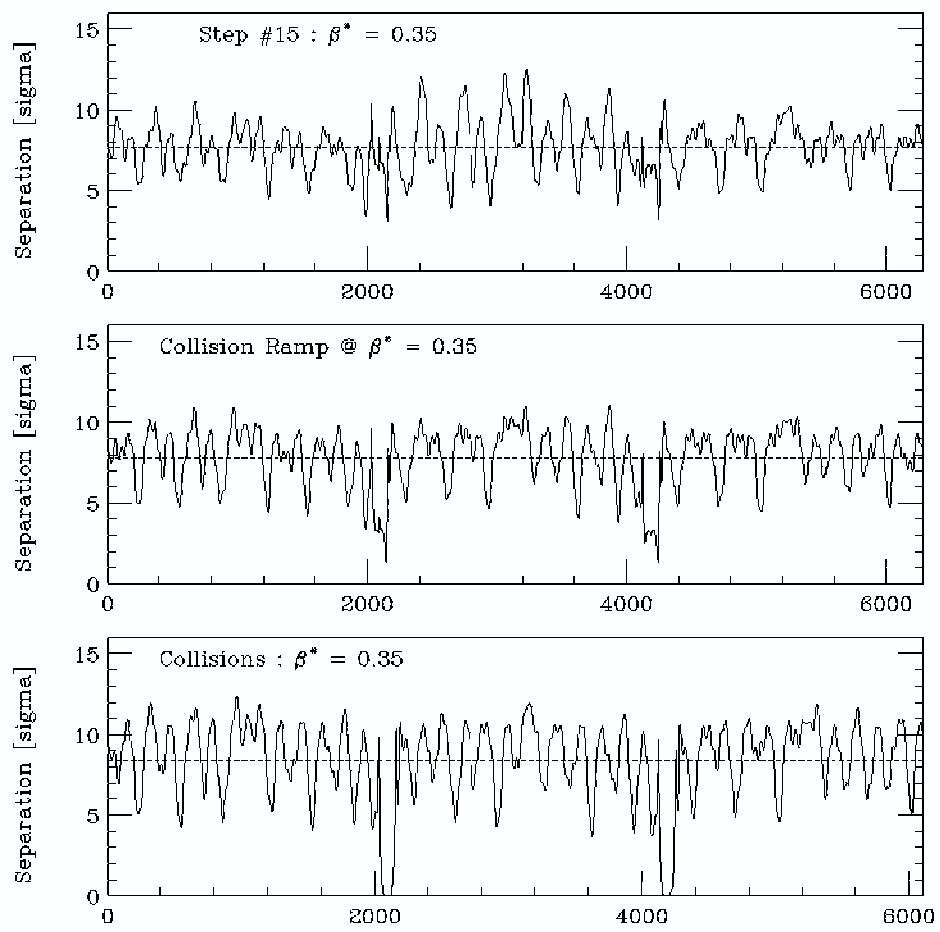

Figure 4. Bringing the beams into collision at Step #15 (β* = 0.35m). Separated beams (top), halfway through the final separator ramp (middle), and collisions (bottom). Average separation in the arcs steadily increases during the ramp, from $\langle\sigma_S\rangle = 7.7$ (top) up to $\langle\sigma_S\rangle = 8.4$ (bottom).

The discussion of improvements to the helix through the low-β squeeze has so far been limited to considering changes that are possible using only the existing, installed separators, and which could therefore be implemented almost immediately. Although there is still considerable room for optimization of this model configuration, it was demonstrated that, even within the limited framework considered, significant increases in beam separation can be acheived.

Subsequent refinements will also explore the benefits of changing the layout and number of separators installed in the ring. Possible upgrade options include installing additional modules at strategic arc locations, and there is also a serious proposal to replace the separators on either side of the IR's with longer modules. Provided that suitable free space locations exist to install more separator modules, the additional kicks could help smooth the helix at all stages of the squeeze. As is discussed more fully in the next section, to replace the D0 IR separators with longer versions would require the experiment to relinquish their Roman Pots to create the necessary space. Without these detectors the constraints on the horizontal orientation of the collision helix also vanish.

This could greatly simplify the manipulations involved in bringing the beams into collision.

5.2 Separation During Collisions

Beam separation during collisions in Run II is currently established with virtually the same configuration of separators as those used in Run I. There are horizontal and vertical separators each side of the IP's, at the A49/B11 and C49/D11 locations, plus an additional separator site in both planes in each of the short and long arcs. With 6 separator locations closed orbit-bumps can be constructed to control position and angle at the IP's while maintaining separated beams everywhere else. The lattice optics are relied upon to keep horizontal and vertical orbits out of phase by $\pi/2$ to create the arc helices.

At 1 TeV and $\beta^* = 0.35$m the beam separation around the ring is illustrated in Fig. 5, showing the center-to-center separation both in terms of mm's and of the transverse beam σ, with the separation in σ defined on the diagonal as:

$$\sigma_S \equiv 2 \cdot \sqrt{\frac{x^2}{\sigma_x^2} + \frac{y^2}{\sigma_y^2}}$$

The corresponding separator gradients are listed in Table 2. The separators each side of the IR's powered to 40 kV/cm correspond to ±100 kV on the plates across a 50mm gap, which is approaching their maximum fields.

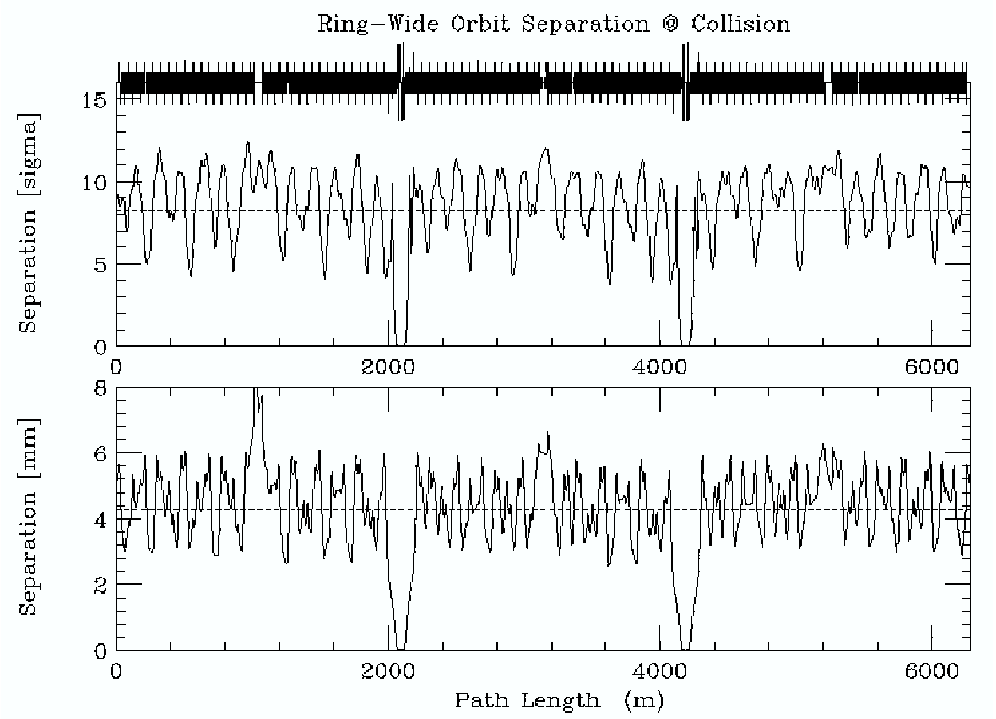

Figure 5. Total p-pbar orbit separation during collisions at 1 TeV and $\beta^* = 0.35$m for 20π μm (95%, normalized) emittance and momentum spread $\delta p/p$=3.375e-4 (95%). Average ring-wide values are indicated by dashed lines.

Separator Gradients (kV/cm)					
Horizontal			Vertical		
A49	1	40.000	A49	2	-32.691
B11	2	40.000	B11	1	40.000
B17	4	-19.042			
			C17	4	-24.352
C49	1	37.070	C49	2	32.796
D11	2	-34.657	D11	1	40.000
D48	1	-5.920			
			A17	1	-16.354

Table 2. Separator gradients for 1 TeV colliding beams.

The beam separations of $\langle\sigma_S\rangle$ = 8.2 and $\langle r_S\rangle$ = 4.3 mm are essentially unchanged from Run I results, with one important exception. With the reduction of bunch spacing to 396 nsec the first near-miss crossing points now occur just 59.275 m from the IP's. This is only ~30m from the IR separators, which is too close for the separators to provide adequate beam separation. Simulations have shown that these 4 points, out of the total of 70 long-range crossings, are responsible for nearly all the long-range beam-beam tune shifts, and are the major driving term of beam-beam odd-order resonances at collision. The separations at these closest crossing points around B0 are shown in Fig. 6. At the first near-miss points the beams are separated by less than a third of the ring-wide average. Precise parameters are provided in Table 3.

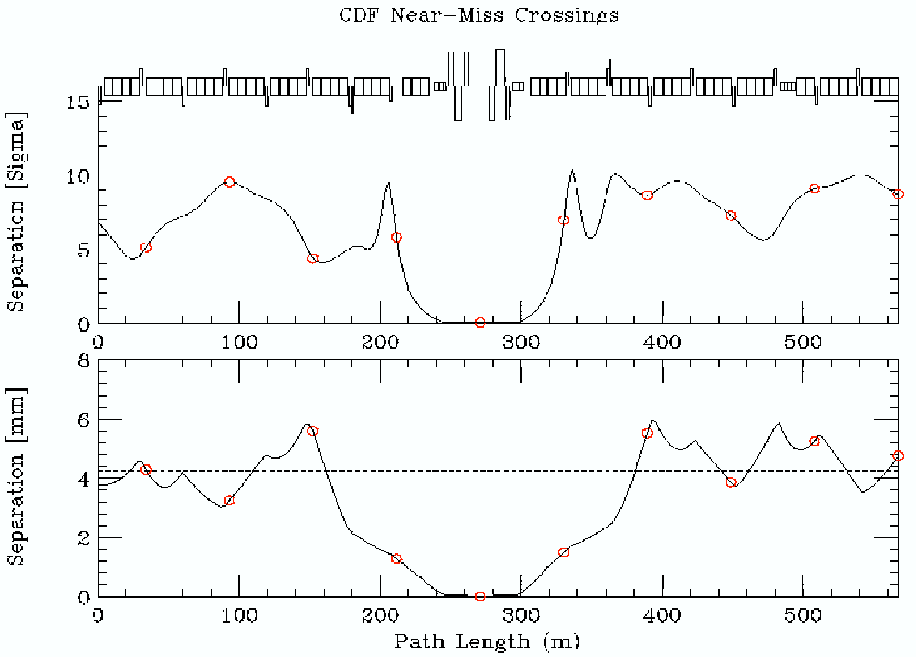

Figure 6. Bunch separation at the parasitic crossings in the vicinity of B0 (circles) during collision of 20π μm, δp/p=3.375e-4 beams. Solid curves denote p-pbar *orbit* separation.

1st Near Misses	Proton Helix								B-B Separation	
	x mm	x' mr	βx m	ηx m	y mm	y' mr	βy m	ηy m	Sep'n σ	Sep'n mm
A48	0.305	-0.010	146.6	0.15	-0.558	0.017	11.63	0.09	5.92	1.27
B0 IP	0.0	0.0	0.35	0.0	0.0	0.0	0.35	0.0	0.0	0.0
B12	0.682	0.021	11.16	0.38	0.305	0.010	153.2	-0.51	6.97	1.49
C48	0.273	-0.009	148.0	-0.23	0.552	-0.017	11.67	0.05	5.83	1.23
D0 IP	0.0	0.0	0.35	0.0	0.0	0.0	0.35	0.0	0.0	0.0
D12	-0.582	-0.018	11.11	0.44	0.301	0.010	151.5	-0.15	5.87	1.31

Table 3. Separation of the p-pbar bunches at the first near-miss points around B0 and D0. Average separations at the 4 locations are just $\langle\sigma_S\rangle = 6.15$ and $\langle r_S\rangle = 1.33$ mm.

The adverse impact of the beam-beam interactions on beam lifetimes and luminosity can be reduced by increasing the p-pbar separation at the long-range crossing points around the ring. While this statement is patently obvious, recent analyses have demonstrated that it is not so simple to assign some simple figure-of-merit to distinguish between the myriad possible separator/helix solutions. Furthermore, while this is not expected to be an issue with the conventional separation solutions considered here, the separation can not simply be increased without bound. Eventually, as the beams probe the higher-order multipole fields away from the magnetic centers the lifetimes will be degraded through diminishing dynamic aperture.

Present plans to modify the separator configuration and helix definition to improve beam separation are proceeding along several lines. Near-term upgrades do not involve new technology and these efforts comprise operational modifications that can be tested and implemented immediately, installation of additional arc separator modules during the next shutdown, and the construction of longer modules for the IR separator locations.

- It is believed that immediate improvements should be possible by increasing the separator voltages in the existing configuration. The separators currently have maximum power supply voltages of 100 - 106 kV, which leads to a spark rate about once every couple of weeks. While the spark rate rises rapidly with voltage, the separators are conditioned to 150 kV and it is speculated that routine voltages as high as 130 kV should be possible without adversely impacting operations. Voltage increases in the existing configuration increase separation uniformly at all crossing points in the ring. Realistic limiting voltages will be determined from operations.

- Improving the separation at primarily the first near-miss points can be accomplished by introducing a small crossing-angle at the IP's. With 6 separator sites in each plane both position and angle at the IP's can be controlled. Now, however, the separator solutions are linked between the long and short arcs. Position control at the IP's in run II is still determined almost entirely by the IR separators at the 49 and 11 locations, and which are also responsible for the bulk of the beam separation in the arcs. Unlike the IP position bumps, there are no obvious, natural separator bump circuits for angular

control at the IP's, and the effect of a crossing-angle extends somewhat into the arcs. Away from the first near-miss points, though, separation at the other 66 crossing points is quickly dominated by the arc separation bumps.

The expression for instantaneous luminosity can be written for particle distributions that are Gaussian in all 3 dimensions as:

$$L = \frac{f \cdot N_1 N_2}{4\pi \cdot \sigma_t^{*2}} \cdot F\left(\beta^*, \theta_{1/2}\right)$$

where f is the revolution frequency, $N_{1,2}$ are the number of particles in a bunch, and σ_t is the rms transverse beam size at the IP ($\beta_x^* = \beta_y^*$, and $\varepsilon_p = \varepsilon_{pbar}$). The form-factor F contains the hour-glass effect and crossing angle information (valid for $|x'^*| = |y'^*|$):

$$F\left(\beta^*, \theta_{1/2}\right) = \frac{2}{\sqrt{\pi}} \cdot z \cdot e^{-z^2\theta_N^2} \cdot \int_0^\infty \frac{du}{1+u^2} \cdot \exp\left[-z^2u^2 + \frac{z^2\theta_N^2}{1+u^2}\right]$$

where θ_N and z are defined in terms of β^*, the total half-crossing angle $\theta_{1/2}$, and the rms bunch length σ_l as:

$$z \equiv \beta^* / \sigma_\ell \qquad \text{and;} \quad \theta_N \equiv \theta_{1/2} \cdot \sigma_\ell / \sigma_t$$

The impact on luminosity of introducing a crossing angle is not insignificant, as demonstrated by Fig. 7, where the decrease of F with crossing-angle is calculated for typical Tevatron beam parameters.

Since the introduction of a crossing angle shortens the luminous region and decreases the instantaneous luminosity, there is a strong incentive to keep the crossing angle as small as possible. In addition to the luminosity degradation, a non-zero crossing angle causes the beams to be separated through the high-gradient IR triplets. The consequences of sending beams off-axis through these magnets is not well understood -- the Tevatron has never been operated before (intentionally) with crossing angles.

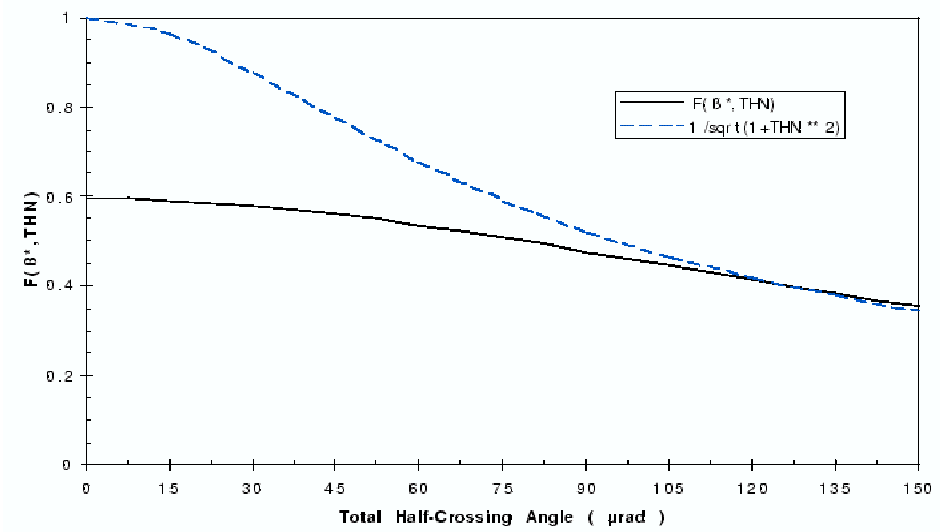

Figure 7. Luminosity variation with total half-crossing angle for $\beta^* = 0.35$m, $\sigma_t^* = 33.1$ μm, and $\sigma_l = 60$ cm. [The dashed curve is the often quoted (but clearly inadequate) approximation to F of $\left(1+\theta_N^2\right)^{-1/2}$, which ignores the impact of the hour-glass effect].

Ultimately, an appropriate crossing angle value will be resolved by operational experience. A priori, this choice is not obvious. The best choice of angle will turn out to be a compromise between the conflicting desires to minimize beam-beam tune shifts without appreciably degrading luminosity.

For this study a total half-crossing angle of $\theta_{1/2} = 50$ μrad ($|x'^*| = |y'^*| = 35$ μrad) was selected, which is less than or comparable to the natural divergence of the beam at the IP. This value creates an additional 22% separation at the first near-miss spots, while inflicting a fairly modest 7% reduction in luminosity:

$$F(0.35m, 50\mu r) \Big/ F(0.35m, 0\mu r) = 0.93$$

The improved separations at the first near-misses are shown in Table 4, and the revised separator gradients for a 50 μrad crossing angle are given in Table 5.

1st Near Misses	Proton Helix								B-B Separation	
	x mm	x' mr	βx m	ηx m	y mm	y' mr	βy m	ηy m	Sep'n σ	Sep'n mm
A48	0.552	0.002	148.4	0.16	-0.629	0.008	11.61	0.09	6.77	1.67
B0 IP	0.0	-0.035	0.35	0.0	0.0	+0.035	0.35	0.0	0.0	0.0
B12	0.624	0.029	11.16	0.38	0.555	-0.001	153.2	-0.50	6.53	1.67
C48	0.530	0.002	147.8	-0.23	0.473	-0.025	11.66	0.05	5.19	1.42
D0 IP	0.0	-0.035	0.35	0.0	0.0	+0.035	0.35	0.0	0.0	0.0
D12	-0.653	-0.009	11.12	0.44	0.548	-0.001	151.8	-0.15	6.70	1.70

Table 4. Improved bunch separation at the near-miss points at B0 and D0. With $\theta_{1/2}$ = 50 μr average separations at the 4 locations are $\langle\sigma_S\rangle$ = 6.30 and $\langle r_S\rangle$ = 1.62 mm.

Separator Gradients (kV/cm)					
Horizontal			Vertical		
A49	1	40.000	A49	2	-33.345
B11	2	40.000	B11	1	40.000
B17	4	-19.314			
			C17	4	-23.847
C49	1	38.161	C49	2	31.606
D11	2	-35.667	D11	1	40.000
D48	1	-22.353			
			A17	1	+5.935

Table 5. Revised separator gradients to create colliding beams with crossing angles at the IP's of |x'*| = |y'*| = 35 μrad. (The A17 voltage is small, but the opposite polarity to the solution without a crossing-angle).

• The Tevatron currently has 4 spare separator modules, and another 4 modules are under construction. As many as 6 out of the 8 will become available for installation in the arcs to improve separation throughout the ring further.

Free space in the Tevatron is extremely limited. In the arcs, for example, magnets completely fill the space between the 17 and 48 locations. Usually the 17 and 48 straights are occupied, too, with separators, collimators, kickers, etc. The long straights are also largely spoken for, containing the 2 detectors, RF, injection/extraction lines, aborts, instrumentation, etc. The BTeV experiment will eventually want to take over the C0 straight (and possibly the B48 location, too). With a single separator module length ~3m, this doesn't leave a lot of locations where additional separators could be installed, but Table 6 lists those sites that could be made available without the application of major surgery and re-design effort.

Available Tevatron Straight Sections			
Location	Space (in)	# ES Modules	Comments
A0	257 349	2 3	Spaces are between each of the abort kickers & abort blocks. Suitable for horizontal separators.
A17	(309)	(2)	Requires moving some or all of the BPM's and Schottky detectors.
B48	347	3	
C0	336 420	2 3	This space will eventually be re-claimed by BTeV.
D17	275	2	
E0	397	3	

Table 6. Tevatron space that is, or can be made, available for additional separator installation.

The gradients for one possible new configuration utilizing the A0, B48, D17 and A17 free spaces are given in Table 7. With the relocation of the D48H separator this solution adds a net total of 6 modules to the ring. The effect of these additional modules is to increase separation by an average of 20% at the 70 long-range interactions. The benefits are not as large as this (11%) for just the 4 near-miss crossings near the IP's. Because of their proximity to the IR's these points are not affected by the installation of new arc separators directly, but only from the increased voltages they permit at 3 out of the 8 IR separator sites.

Separator Gradients (kV/cm)					
Horizontal			Vertical		
A49	1	40.000	A49	2	-40.000
B11	2	40.000	B11	1	40.000
B17	4	-19.042			
			B48	2	20.919
			C17	4	-27.906
C49	1	37.070	C49	2	40.000
D11	2	-40.000	D11	1	40.000
			D17	2	-34.381
A0U	1	5.897			
A17	1	-20.857	A17	1	-30.912

Table 7. Improved separator configuration using 6 additional arc modules.

The solution given here has been optimized to produce the greatest gains in the long arc during collision. Separation improvements through the short arc are not as simple to obtain. Vertical separation is significantly increased with the addition of new separators at B48. However, in the horizontal plane, neither the B48 site nor the C0 straight has the appropriate phase advance to make a noticeable impact on beam separation. Further study

is needed to determine if the new separator locations chosen will also improve the helix at injection and during the acceleration ramp.

• The IR optics of Run II are not the same as those from Run I. In re-powering the IR quadrupole circuits to produce an $\eta^* = \eta'^* = 0$ solution at the IP's the high-gradient 55" Q1 magnets became unnecessary. (These magnets are situated between the arc dipoles and outboard ends of the separators). Although the Q1 magnets are now irrelevant, the accompanying P-spools contain dipole correctors and BPM's in both planes plus a skew quadrupole and 5000 A power lead. These valuable elements can not simply be discarded in the quest for additional separator space. Removing the Q1 magnets frees 72.827" of space. If the P-spools are also replaced with shorter H-spools (which are missing the horizontal BPM) an additional 6.239" is generated. By replacing the Q1 plus P-spool combination with an H-spool the electrode plates of the 3 separator modules each side of the IP could comfortably be extended by 24" from the 101.25" of the existing separator design.

There is no benefit derived from installing longer separators only at B0. In this case the beam separation in the arcs would still be determined by the gradients of the shorter, standard separators at D0. New separators must be installed at the 49/11 locations of both B0 and D0 to be useful. Unfortunately, D0 has already removed the Q1 magnets to create room for their Roman pots. Longer separators means that these detectors would have to be discarded. Assuming that this is acceptable, gradients for the new helix are given in Table 8. The overall gain is a 19% increase in average separation around the ring.

Separator Gradients (kV/cm)					
Horizontal			Vertical		
A49	1	40.000	A49	2	-31/933
B11	2	40.000	B11	1	40.000
B17	4	-23.012			
			C17	4	-29.020
C49	1	37.569	C49	2	32.510
D11	2	-34.178	D11	1	40.000
D48	1	-6.208			
			A17	1	-21.078

Table 8. Gradients with the twelve A49/B11 and C49/D11 electrodes extended by 24" each.

The expected impacts of the 4 separator upgrades just discussed on beam separation are summarized in Table 9, and the resulting ring-wide separation is illustrated in Figure 8.

Modifications for Increased Beam Separation	Near-Misses Gain (%)	Ring-Wide Gain (%)
10% Separator Voltage Increase	10.0	10.0
50 μrad Half-Crossing Angle	21.5	≈0
Additional Arc Modules	7.7	15.0
Increased IR Separator Lengths	19.0	19.0
Total Separation Gain	71.3 %	50.5 %

Table 9. Beam separation improvements from modest helix upgrades.

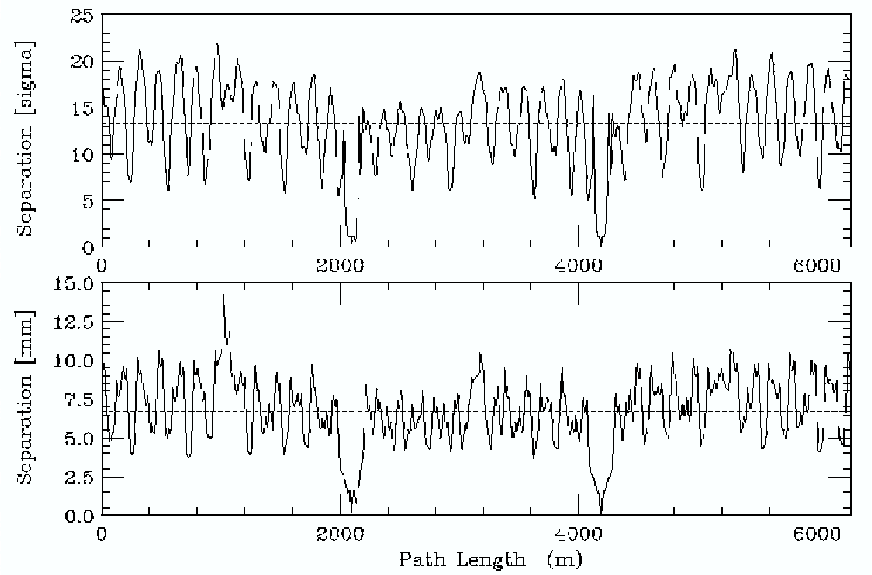

Figure 8. Orbit separation during collisions with separator configuration upgrades. Average ring-wide values are increased to $\langle\sigma_S\rangle$ = 13.33 and $\langle r_S\rangle$ = 6.66 mm. (*c.f.* Figure 5).

The beam separation upgrade path discussed in this section was considered with an eye to being able to implement changes within the near future. Even the construction of longer separator modules is not seen to present any new engineering challenges, as they are imagined to be simply stretch versions of the existing design. Beyond these improvements, any futher modifications will require an R&D commitment. One possibility being considered is to build new modules of a better design. Results from other laboratories suggest that significantly higher gradients can be obtained using cathodes constructed from materials other than stainless steel (as in the existing Tevatron units). A test bed is currently being prepared to study the behavior of electrodes coated with a variety of materials, including aluminum oxide and semi-conducting glass.